Role of Surface-Segregation-Driven Intermixing on the Thermal Transport through Planar Si/Ge Superlattices

Peixuan Chen,[1,2,*] N. A. Katcho,[3] J. P. Feser,[4] Wu Li,[3] M. Glaser,[2] O. G. Schmidt,[1] David G. Cahill,[4] N. Mingo,[3,†] and A. Rastelli[1,2,‡]

[1]*Institute for Integrative Nanosciences, IFW Dresden, Helmholtzstrasse 20, 01069 Dresden, Germany*
[2]*Institute of Semiconductor and Solid State Physics, Johannes Kepler University Linz, Altenbergerstrasse 69, A-4040 Linz, Austria*
[3]*LITEN, CEA-Grenoble, 17 Rue des Martyrs, 38054 Grenoble Cedex 9, France*
[4]*Department of Materials Science and Engineering, Materials Research Laboratory, University of Illinois at Urbana-Champaign, Urbana, Illinois 61801, USA*
(Received 24 January 2013; published 9 September 2013)

It has been highly debated whether the thermal conductivity κ of a disordered SiGe alloy can be lowered by redistributing its constituent species so as to form an ordered superlattice. By *ab initio* calculations backed by systematic experiments, we show that Ge segregation occurring during epitaxial growth can lead to κ values not only lower than the alloy's, but also lower than the perfect superlattice values. Thus we theoretically demonstrate that κ does not monotonically decrease as the Si- and Ge-rich regions become more sharply defined. Instead, an intermediate concentration profile is able to lower κ below both the alloy limit (total intermixing) and also the abrupt interface limit (zero intermixing). This unexpected result is attributed to the peculiar behavior of the phonon mean free path in realistic Si/Ge superlattices, which shows a crossover from abrupt-interface- to alloylike values at intermediate phonon frequencies of ~3 THz. Our calculated κ's quantitatively agree with the measurements when the realistic, partially intermixed profiles produced by segregation are considered.

DOI: 10.1103/PhysRevLett.111.115901 PACS numbers: 66.70.Df, 64.75.Nx, 68.55.ag, 68.65.Cd

Understanding the effects produced by nanostructuring and interfaces on thermal transport is important for heat management in nano- and optoelectronics and for the development of thermoelectric materials and devices with improved efficiency [1–4]. SiGe-based superlattices (SLs) are an ideal platform to study the effects of nanostructuring on thermal transport, as they consist of only two elements. Moreover, they are appealing from a practical point of view, as they can be monolithically integrated on Si substrates for possible microcooling and energy harvesting applications [3,5]. Although SiGe-based SLs and interfaces have been extensively used for theoretical studies [6–16], experiments on planar SiGe SLs are still limited [17–21] and a clear picture of how their cross-plane thermal conductivity κ depends on SL structural parameters is still missing. This has recently led Cheaito *et al.* [22] to argue that the κ's of SiGe SLs are ultimately limited by the total SL thickness rather than by relevant parameters, such as period length, and to doubt whether SLs can achieve κ's below those of SiGe alloy films with the same average Ge concentration and thickness. This unsatisfactory state-of-the-art is partially due to crystal defects, which arise from strain relaxation in relatively thick layers due to the lattice mismatch between Si and Ge, and which have plagued the interpretation of most results so far [17,18,20].

In this Letter we assess, via systematic experiments on defect-free SLs and atomistic *ab initio* calculations, how the periodic concentration modulation in SLs affects the κ of single-crystalline SiGe. We show not only that κ of SLs decreases below the homogeneous alloy values, but, more importantly, that redistributing Si and Ge into pure layers separated by sharp interfaces does not produce the lowest possible κ, and lower values are obtained in realistic SLs with partly intermixed profiles resulting from Ge segregation during growth. A clear signature of this phenomenon is observed in the dependence of κ with Ge thickness, which is noticeably different from the one expected for the homogeneous and the sharp-interface profiles. By including for the first time the realistic Si-Ge distribution into the calculations, we find good quantitative agreement with the experiments and demonstrate that the low κ's of real SLs are linked to their capability of scattering high-frequency phonons as efficiently as the corresponding alloy and low-frequency phonons as SLs with abrupt interfaces. Finally, we demonstrate defect-free SLs with κ's below the alloy values even considering the reduction of alloy κ produced by finite film-thickness effects [22].

Experiments were performed on $(Si)_m/(Ge)_n$ SLs grown by molecular beam epitaxy (MBE) on Si(001) wafers at a substrate temperature of 500 °C. SLs consist of N periods of n monolayers (ML) of Ge (''barrier'') separated by m ML of Si (''spacer''), as sketched in Fig. 1(a). All parameters were systematically varied in a wide range to reach a clear picture of their impact on κ. The actual SL thicknesses of selected samples were quantified by x-ray diffraction and transmission electron microscopy. Samples can be considered dislocation-free unless otherwise stated. To assess whether SLs are planar or contain nanodots

 © 2013 American Physical Society

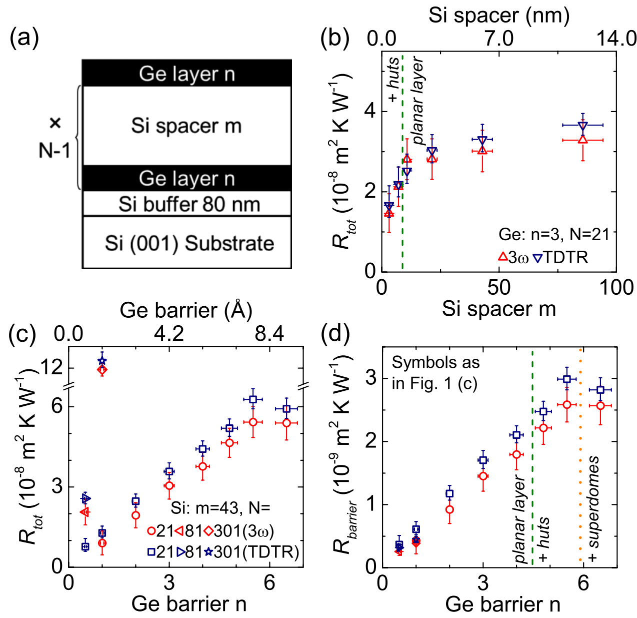

FIG. 1 (color online). (a) Sketch of the $(\mathrm{Si})_m/(\mathrm{Ge})_n$ SL structures. (b) Total thermal resistance R_{tot} of SLs with fixed Ge amount per layer (3 ML) and variable Si-spacer thickness. The Ge period number N is 21. (c) Total thermal resistance and (d) single-barrier thermal resistance as a function of Ge-layer thickness of SLs with fixed Si-spacer thickness (43 ML). Different symbols are used for the results obtained by 3ω and TDTR methods. The vertical dashed and dotted lines in (b) and (d) separate regions of planar SLs, SLs with coherently strained nanodots (huts) and SLs with dislocated nanodots (superdomes). All measurements were performed at room temperature.

(with "hut" shape [23,24] for our growth conditions), the surface morphology of all samples was characterized by atomic force microscopy (AFM).

The cross plane κ of the SLs was measured independently with the differential 3ω method [25,26] and with time-domain thermoreflectance (TDTR) [27,28] at room temperature, providing compatible results within the uncertainties (see Supplemental Material [29]). Figure 1(b) shows the thermal resistance R_{tot} (i.e., the ratio of total SL thickness and κ) of SLs with variable Si-spacer thickness and fixed Ge-barrier thickness (3 ML) and period number ($N = 21$). R_{tot} increases slowly when $m \gtrsim 10$, indicating that the Si spacer has only a minor effect on R_{tot}. This finding is in line with previous results on nanodot SLs [30], which were interpreted as due to the quasiballistic transport of phonons in the Si spacer followed by scattering at the Ge barriers.

A much stronger dependence on the Ge-barrier thickness and period number N is observed in Fig. 1(c), which displays R_{tot} vs n for $(\mathrm{Si})_{43}/\mathrm{Ge}_n$ SLs. From Fig. 1(d) we see that SLs which differ only in N have the same value of "barrier resistance", $R_{\mathrm{barrier}} = R_{\mathrm{tot}}/N$. In other words, the SLs can be seen as series of N thermal resistors and their κ's *do not show* any significant dependence on the total film thickness [see also Fig. 2(a)]. This observation, which contrasts with the recent conjectures of Ref. [22], indicates that phonon transport in our SLs is mostly incoherent. Most interestingly, Fig. 1(d) demonstrates a smooth linear increase of R_{barrier} with n. Only for $n \gtrsim 6$, does R_{barrier} saturate and show a slight drop. AFM images of this sample reveal the presence of plastically relaxed dots ("superdomes"), with surface densities of $\sim 3 \times 10^8\ \mathrm{cm}^{-2}$. The resistance decrease is at first surprising, as one may expect the crystal defects to contribute to phonon scattering. However superdomes also act as sinks for Ge adatoms [31], as they have lower surface chemical potential compared to coherently strained regions. The drop in R_{barrier} thus means that redistributing Ge into superdomes *increases* κ and that the effective Ge-barrier thickness cannot be increased significantly beyond $\sim$6 ML.

Figures 2(a) and 2(b) show the κ's corresponding to the data displayed in Figs. 1(c) and 1(b). Many previous investigations on Si-Ge SLs [10,12–14,18–20] have focused on the effect of the period length L on κ. However, it may be misleading to compare the κ of different SLs based only on such a quantity, as κ decreases [Fig. 2(a)] or increases [Fig. 2(b)] with $L \simeq (n + m)$ ML, depending on whether we increase the thickness of the Ge or Si layers. (This is the reason for referring to Ge and Si as barrier and spacer). Remarkably, the average Ge concentration for the SLs considered in Fig. 2(a) is very low (see top axis of the plot), indicating that this kind of SL is very effective in achieving low κ's (down to $\sim$2.3 W/m·K). When we

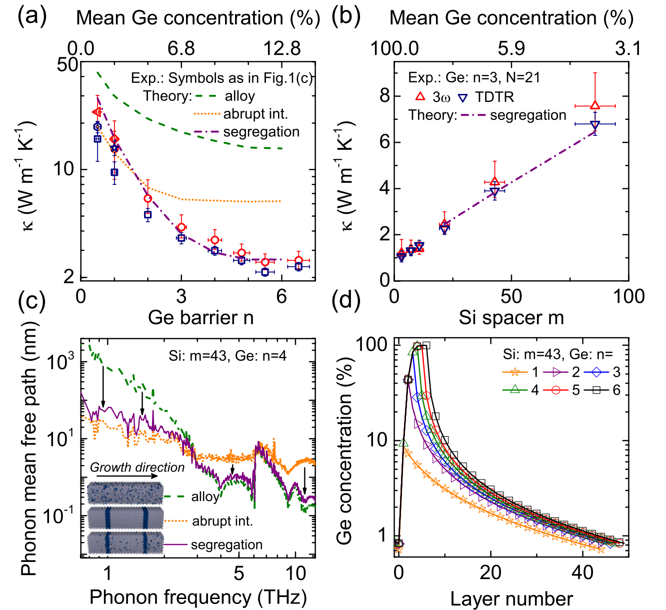

FIG. 2 (color online). (a) Comparison of experimental and theoretical cross-plane κ for $(\mathrm{Si})_{43}/(\mathrm{Ge})_n$ SLs. (b) Comparison of experimental and theoretical κ for $(\mathrm{Si})_m/(\mathrm{Ge})_3$ SLs. N is the period number. (c) Calculated phonon mean free path spectrum for the $(\mathrm{Si})_{43}/(\mathrm{Ge})_4$ SL with (solid line) and without (dotted line) Ge segregation and the corresponding alloy (dashed line). The structure models used for *ab initio* calculations are illustrated in the inset. (d) Expected concentration profiles of a single SL period for different $(\mathrm{Si})_{43}/(\mathrm{Ge})_n$ SLs, according to the model in Ref. [37].

decrease m down to 3 (with $n = 3$), κ decreases down to $\sim 1.2\ \mathrm{W/m \cdot K}$ [Fig. 2(b)]. Obviously κ cannot be indefinitely reduced by simply decreasing the Si spacer thickness, since in the limit of $m = 0$ we expect κ to coincide with the value of a Ge film. In fact, Fig. 1(b) displays a steep drop of R_{tot}, related to the thermal conductivity by $\kappa \sim NL/R_{\mathrm{tot}}$, when $m \lesssim 10$.

To understand the experimental results, we computed the thermal conductivity κ by solving the Boltzmann transport equation from first principles. Some of us have recently presented a related method as applied to embedded nanoparticles [32,33]. In the present case, calculation of the scattering rates is complicated by the geometry of the planar scatterers. We first consider the ideal Si/Ge distribution resulting from the sequential deposition of n ML of Ge followed by m ML of Si, i.e., SLs with abrupt interfaces [see central sketch in the inset of Fig. 2(c), and calculation details in the Supplemental Material [29]]. The calculated κ is shown as a dotted line in Fig. 2(a). Whereas κ for thin barriers ($n \leq 2$) is in agreement with experimental values, the one for thicker barriers ($n > 2$) is considerably *above the experiment*, settling to a constant value instead of continuing to decrease with increasing n. Qualitatively, this saturation is related to the fact that, when a sharp homogeneous barrier becomes much thicker than the phonon wavelength, the averaged transmission in one dimension can be written in terms of the individual transmissions of its two interfaces, independent of the thickness [34].

Simplistically, one might have expected that the alternation of pure Ge and Si layers led to the lowest κ due to the highest acoustic mismatch at the interfaces. It is thus surprising to find that the experimental κ's are lower than the theoretical values considering that interfaces in real SLs are not abrupt mainly because of Ge segregation [35–38], i.e., the tendency of Ge adatoms to float on the surface during Si overgrowth, which causes intermixing of Ge into the Si spacers. To simulate the thermal response of the experimental SLs, we retrieve the realistic Ge concentration profiles using the kinetic model proposed by Godbey and Ancona [37]. This model and related parameters (activation energies) are based on experimental results obtained on SiGe samples grown using the same method (MBE) and same nominal substrate temperature (500 °C) as ours. The expected concentration profiles are shown in Fig. 2(d) and in the bottommost sketch in the inset of Fig. 2(c). The calculated κ's shown by the dot-dashed line in Fig. 2(a) are now in very good quantitative agreement with the measured ones. As in the experiment, κ keeps decreasing as the Ge-layer thickness is increased, and saturates only beyond 5 ML. Thus, a very dilute amount of Ge (less than 5% on average), segregated into the Si spacers, can considerably decrease κ below the sharp barrier case, and also below the homogeneous alloy case [complete interdiffusion, see topmost sketch in the inset of Fig. 2(c)]. The latter is shown as a dashed line in Fig. 2(a).

The physical reason behind the remarkable performance of real SLs in scattering phonons is evident when comparing the spectral dependence of the phonon mean free path (MFP) for different Ge concentration profiles, as illustrated in Fig. 2(c) for Si_{43}/Ge_4 SLs and the corresponding alloy. Compared to an alloy, the ideal Si/Ge SL with pure layers (dotted line) shows higher scattering efficiency for phonons with low frequency (less than $\sim$3 THz in the example) while the alloy (dashed line) is superior at higher frequencies. Realistic SLs, which are characterized by graded Ge profiles (solid line) bring together the advantages of the two extremes: their MFPs almost coincide with the ideal SL's values at low frequency and with the alloy's at high frequency, resulting in enhanced scattering at all frequencies and a smaller κ. In other words, alloying lowers the MFP of a SL and layering lowers the MFP of an alloy (see black arrows in Fig. 2(c)). The multiscale scattering behavior of our segregated SLs strongly differs from that of nanodots in a matrix [39,40] because of their dimensionality and the physics at play. The technical approach and difficulties of the calculation are also different, since planar superlattices require a hybrid real-reciprocal space description. Whereas embedded nanodots are inherently different from the matrix, our planar SLs only involve Si and Ge, which allow for a cleaner interpretation and modeling. Indeed, while no quantitative *ab initio* calculation appears to have been published on nanodot systems, our fully *ab initio* calculations agree quantitatively with the experimental data, as it is also apparent in the case of fixed Ge thickness (3 ML) and variable thickness of Si spacer [see Fig. 2(b)] [41].

We now compare the κ's of our $(Si)_m/(Ge)_n$ SLs and that of bulk $Si_{1-x}Ge_x$ alloys with the same average Ge concentration [$x \sim n/(n+m)$]. Figure 2(a) shows that the calculated κ's of SLs (both with and without interdiffusion) are substantially lower than the κ values of the corresponding alloys. This is further illustrated by Fig. 3(a), which displays the experimental κ's of our SLs together with those of bulk alloys [42,43] and also previous experimental reports on planar and nanodot SLs [17–19,21,30,44–49]. Not only do our SLs lie below the alloy values but also below most of the previous results on SiGe SLs. [Data affected by defects in Ref. [17] are not included in Fig. 3(a).] In addition, the κ of our SLs decreases much faster with x compared with diluted SiGe alloys. We quantify this observation by fitting the κ vs x data in the range between 0.01 and 0.1 with a simple power law. While for bulk alloys we obtain $\kappa_{\mathrm{alloy}} \propto x^{-0.5}$, our SLs yield $\kappa_{\mathrm{SL}} \propto x^{-1}$, providing experimental evidence that distributing Ge into a SL configuration is more effective than homogeneous alloying in lowering the κ of the resulting SiGe-based material. The alloy power dependence can be easily derived analytically as follows. Assuming a Debye model for the phonon density of states, $\kappa_{\mathrm{alloy}}(T) \propto \int_0^{\nu_D} \nu^2 \tau(\nu) d\nu$, where ν_D is the Debye frequency. At low (high) frequencies the anharmonic (mass disorder) scattering dominates. Assuming a low Ge concentration, so that

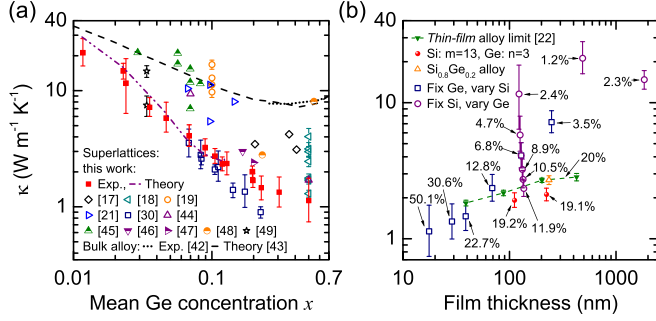

FIG. 3 (color online). κ of $(\mathrm{Si})_m/(\mathrm{Ge})_n$ SLs as a function of (a) mean Ge concentration $x \sim n/(n+m)$ and (b) total film thickness. The thermal conductivities are obtained by averaging the 3ω and TDTR results. Our theory results as well as bulk alloy and SL data from the indicated Refs. are also included in (a). κ's for thin $\mathrm{Si}_{0.8}\mathrm{Ge}_{0.2}$ alloy films from Ref. [22] (“*thin-film* alloy limit”) and the TDTR measurement of an alloy film grown in this work are shown in (b). In (b) the mean Ge concentration is indicated near each data point.

$x(1-x) \sim x$, the corresponding scattering rates are $\tau_{\mathrm{anh}}^{-1} \propto T\nu^2$ and $\tau_{\mathrm{mass}}^{-1} \propto x\nu^4$. Then κ_{alloy} can be approximated as $\kappa_{\mathrm{alloy}} \propto \int_0^{\nu_1} \nu^2 \tau_{\mathrm{anh}}(\nu) d\nu + \int_{\nu_1}^{\nu_D} \nu^2 \tau_{\mathrm{mass}}(\nu) d\nu$, where ν_1 is the frequency at which $\tau_{\mathrm{anh}}^{-1} = \tau_{\mathrm{mass}}^{-1}$. Assuming that $\nu_1 \ll \nu_D$, as it must be if the alloy disorder strongly influences κ, one finds $\kappa_{\mathrm{alloy}} \propto x^{-0.5}$. In the case of a SL A_n/B_m, a reasonable approximation is to describe the SL scattering rate as $\tau_{\mathrm{SL}}^{-1} = (\tau_l + \tau_s)^{-1}$, where τ_l^{-1} and τ_s^{-1} are rates for the long- and short-wavelength limits [50]. τ_l^{-1} corresponds to the Rayleigh regime, which for a SL is $\tau_l^{-1} \propto n^2\nu^2/(n+m)$. τ_s^{-1} corresponds to the geometrical limit, where the cross section is independent of ν, and τ_s^{-1} depends only on the number of barriers per unit volume, i.e., $\tau_s^{-1} \propto 1/(n+m)$. For the case of constant barrier thickness (n) and variable spacer thickness (m), it is easy to find that both τ_l and τ_s, and hence κ_{SL}, are proportional to x^{-1}, in agreement with our experimental results [Fig. 3(a)]. However when m is constant, we find $\tau_l^{-1} \propto x^2\nu^2$ and τ_s^{-1} constant, leading to $\kappa_{\mathrm{SL}} \propto a + b/x^2$, with a (b) related with the geometrical (Rayleigh) regimes. The two limiting cases correspond to all the scattering being described by the geometrical regime or by the Rayleigh one, i.e., to a mass difference between the barrier and the spacer which tends to ∞ or 0. For the first case, the exponent α in the $\kappa_{\mathrm{SL}} \propto x^\alpha$ tends to zero while for the second one it tends to -2. It is thus not possible to give a universal value for α in the SL case, as it depends on factors, such as the magnitude of the mass difference and the concentration profile. The scatter observed in the previous data shown in Fig. 3(a) is in line with this conclusion. It is thus evident that *ab initio* calculations using realistic concentration profiles presented here are necessary for a quantitative description of thermal transport. For the particular case of segregated Si/Ge superlattices investigated here, we find both experimentally and theoretically a value close to -1 [see filled squares and the dot-dashed line in Fig. 3(a)].

As recently stressed in Ref. [22], the comparison between thin-film measurements and bulk values may be misleading, as κ may depend also on the total film thickness [51]. In fact, it was shown that κ for a $\mathrm{Si}_{1-x}\mathrm{Ge}_x$ alloy thin film with $x \sim 20\%$ and thickness of $\sim$39 nm can be as low as $\sim$1.8 W/m $\cdot$ K because of scattering of low frequency phonons at the interface between the SiGe film and Si substrate. As already mentioned, and in contrast to alloys, the κ of all the SLs we measured so far appears independent of their total film thickness. We tentatively ascribe the different behavior to the fact that our Si/Ge SLs also scatter efficiently low frequency phonons; see Fig. 2(c). In other words, the interface between the Si substrate and the SL plays a minor role compared to the many interfaces already present in the SL. To test nevertheless whether our SLs can beat the “thin-film alloy limit” [22], we have grown $(\mathrm{Si})_{13}/(\mathrm{Ge})_3$ SLs ($x \sim 19\%$) with $N = 51$ and 101 and a reference $\mathrm{Si}_{0.8}\mathrm{Ge}_{0.2}$ film (at the same substrate temperature of 500 °C). Their κ's are shown in Fig. 3(b) vs film thickness together with all samples presented here, as well as the alloy data from Ref. [22]. While the κ of our alloy film is compatible with previous measurements, the κ of the SL with $N = 101$ (which is still defect-free), is about three standard deviations below the values reported for *dislocated* alloy films in Ref. [22], confirming that the reduction of κ does stem from the SL structure and not from the limited film thickness.

In conclusion, planar superlattices with sharp interfaces are not the most efficient structures to decrease a materials' κ below the alloy limit. Much lower κ's can be achieved by virtue of the partial intermixing that naturally occurs due to segregation during growth. This phenomenon enables us to obtain thermal conductivities that are 5 and 3 times lower than the alloy and sharp-barrier limits, respectively. Using two different characterization techniques and carefully grown superlattices, we have demonstrated such thermal conductivities and their tunability in a wide range of barrier and spacer thicknesses. Atomistic *ab initio* simulations using realistic concentration profiles have elucidated the crucial role of segregation-driven intermixing in lowering the conductivity below what could be expected for SLs with abrupt interfaces. The results presented are expected to be relevant to many applications requiring optimization of thermal transport in SL structures [2,3,52].

We are grateful to V. Fomin, D. Nika, and A. Cocemasov for fruitful discussions, J. J. Zhang, D. J. Thurmer, G. Chen, and F. Schäffler for assistance with the MBE growth, T. Etselstorfer and J. Stangl for x-ray diffraction measurements, G. Bernard-Granger, V. Delaye, H. T. Chang, and S. W. Lee for transmission electron microscopy measurements, I. Daruka for fruitful discussions on the calculation of Ge profiles, D. Grimm, I. Mönch, A. Halilovic, G. Katsaros, U. Kainz, and S. Bräuer for assistance with processing samples for the 3ω measurements, D. A. Broido, D. A. Stewart, and L. Lindsay for fruitful discussions on the *ab initio* approach. This work was supported by the SPP1386 (RA 1634/5-1), EU FP7 (NEAT, Grant

No. 263440), CEA (THERMA), ANR-08-NANO-P132-48 (ACCATTONE), and the EFRE program. TDTR measurements at the University of Illinois were supported by the US Air Force Office of Scientific Research (AFOSR) Multidisciplinary University Research Initiative Grant No. FA9550-08-1-0407.

*peixuan.chen@jku.at
†natalio.mingo@cea.fr
‡armando.rastelli@jku.at

[1] D. G. Cahill, W. K. Ford, K. E. Goodson, G. D. Mahan, A. Majumdar, H. J. Maris, R. Merlin, and S. R. Phillpot, J. Appl. Phys. **93**, 793 (2003).
[2] Y. Bai, S. Slivken, S. Kuboya, S. R. Darvish, and M. Razeghi, Nat. Photonics **4**, 99 (2010).
[3] A. Shakouri, Proc. IEEE **94**, 1613 (2006).
[4] G. J. Snyder and E. S. Toberer, Nat. Mater. **7**, 105 (2008).
[5] D. J. Paul *et al.*, *Proceedings of the 12th IEEE International Conference on Nanotechnology 2012* (IEEE, New York, 2012), p. 1–5.
[6] P. Hyldgaard and G. D. Mahan, Phys. Rev. B **56**, 10754 (1997).
[7] G. Chen, Phys. Rev. B **57**, 14958 (1998).
[8] A. A. Kiselev, K. W. Kim, and M. A. Stroscio, Phys. Rev. B **62**, 6896 (2000).
[9] H. Zhao and J. B. Freund, J. Appl. Phys. **97**, 024903 (2005).
[10] E. S. Landry and A. J. H. McGaughey, Phys. Rev. B **79**, 075316 (2009).
[11] E. S. Landry and A. J. H. McGaughey, J. Appl. Phys. **107**, 013521 (2010).
[12] J. Garg, N. Bonini, and N. Marzari, Nano Lett. **11**, 5135 (2011).
[13] G. Balasubramanian and I. K. Purl, Appl. Phys. Lett. **99**, 013116 (2011).
[14] Y. Chalopin, K. Esfarjani, A. Henry, S. Volz, and G. Chen, Phys. Rev. B **85**, 195302 (2012).
[15] X. Li and R. G. Yang, Phys. Rev. B **86**, 054305 (2012).
[16] Z. Tian, K. Esfarjani, and G. Chen, Phys. Rev. B **86**, 235304 (2012).
[17] S.-M. Lee, D. G. Cahill, and R. Venkatasubramanian, Appl. Phys. Lett. **70**, 2957 (1997).
[18] T. Borca-Tasciuc *et al.*, Superlattices Microstruct. **28**, 199 (2000).
[19] S. T. Huxtable, A. R. Abramson, C.-L. Tien, A. Majumdar, C. LaBounty, X. Fan, G. Zeng, J. E. Bowers, A. Shakouri, and E. T. Croke, Appl. Phys. Lett. **80**, 1737 (2002).
[20] S. Chakraborty, C. A. Kleint, A. Heinrich, C. M. Schneider, J. Schumann, M. Falke, and S. Teichert, Appl. Phys. Lett. **83**, 4184 (2003).
[21] C.-K. Liu, C-K. Yu, H.-C. Chien, S.-L. Kuo, C.-Y. Hsu, M.-J. Dai, G.-L. Luo, S.-C. Huang, and M.-J. Huang, J. Appl. Phys. **104**, 114301 (2008).
[22] R. Cheaito; J. C. Duda, T. E. Beechem, K. Hattar, J. F. Ihlefeld, D. L. Medlin, M. A. Rodriguez, M. J. Campion, E. S. Piekos, and P. E. Hopkins, Phys. Rev. Lett. **109**, 195901 (2012).
[23] O. G. Schmidt, C. Lange, and K. Eberl, Appl. Phys. Lett. **75**, 1905 (1999).
[24] Y. W. Mo, D. E. Savage, B. S. Swartzentruber, and M. G. Lagally, Phys. Rev. Lett. **65**, 1020 (1990).
[25] D. G. Cahill, Rev. Sci. Instrum. **61**, 802 (1990).
[26] D. G. Cahill, M. Katiyar, and J. R. Abelson, Phys. Rev. B **50**, 6077 (1994).
[27] C. A. Paddock and G. L. Eesley, J. Appl. Phys. **60**, 285 (1986).
[28] D. G. Cahill, Rev. Sci. Instrum. **75**, 5119 (2004).
[29] See Supplemental Material at http://link.aps.org/supplemental/10.1103/PhysRevLett.111.115901 for surface morphology of the grown superlattices and details on the methods used to measure and calculate their thermal conductivity.
[30] G. Pernot *et al.*, Nat. Mater. **9**, 491 (2010).
[31] M. Stoffel, A. Rastelli, J. Tersoff, T. Merdzhanova, and O. G. Schmidt, Phys. Rev. B **74**, 155326 (2006).
[32] A. Kundu, N. Mingo, D. A. Broido, and D. A. Stewart, Phys. Rev. B **84**, 125426 (2011).
[33] N. A. Katcho, N. Mingo, and D. A. Broido, Phys. Rev. B **85**, 115208 (2012).
[34] N. Mingo, L. Yang, J. Han, and M. P. Anantram, Phys. Status Solidi B **226**, 79 (2001).
[35] S. S. Iyer, J. C. Tsang, M. W. Copel, P. R. Putike, and R. M. Tromp, Appl. Phys. Lett. **54**, 219 (1989).
[36] K. Nakagawa and M. Miyao, J. Appl. Phys. **69**, 3058 (1991).
[37] D. J. Godbey and M. Ancona, J. Vac. Sci. Technol. A **15**, 976 (1997).
[38] A. Rastelli, H. Von Känel, G. Albini, P. Raiteri, D. B. Migas, and L. Miglio, Phys. Rev. Lett. **90**, 216104 (2003).
[39] W. Kim, J. Zide, A. Gossard, D. Klenov, S. Stemmer, A. Shakouri, and A. Majumdar, Phys. Rev. Lett. **96**, 045901 (2006).
[40] K. Biswas, J. He, I. D. Blum, C.-I. Wu, T. P. Hogan, D. N. Seidman, V. P. Dravid, and M. G. Kanatzidis, Nature (London) **489**, 414 (2012).
[41] Although the Ge amount per layer (3 ML) is well below the critical thickness (~ 4.7 ML) for dot formation on Si (001), surface segregation leads to Ge floating on the surface of the Si spacers, so that nanodots are observed when $m < 10$ (see AFM images in the Supplemental Material [29]). For this reason, we have not performed calculations for structures with $m < 10$, as nanodots would need to be treated differently than the planar barriers considered here. Developing such a model is beyond the scope of this Letter.
[42] J. P. Dismukes, L. Ekstrom, E. F. Steigmeier, I. Kudman, and D. S. Beers, J. Appl. Phys. **35**, 2899 (1964).
[43] J. Garg, N. Bonini, B. Kozinsky, and N. Marzari, Phys. Rev. Lett. **106**, 045901 (2011).
[44] W. L. Liu, T. Borca-Tasciuc, G. Chen, J. L. Liu, and K. L. Wang, J. Nanosci. Nanotechnol. **1**, 39 (2001).
[45] J. L. Liu, A. Khitun, K. L. Wang, W. L. Liu, G. Chen, Q. H. Xie, and S. G. Thomas, Phys. Rev. B **67**, 165333 (2003).
[46] B. Yang, J. L. Liu, K. L. Wang, and G. Chen, Appl. Phys. Lett. **80**, 1758 (2002).
[47] B. Yang, W. L. Liu, J. L. Liu, K. L. Wang, and G. Chen, Appl. Phys. Lett. **81**, 3588 (2002).
[48] Y. Ezzahri, S. Dilhaire, S. Grauby, J. M. Rampnoux, W. Claeys, Y. Zhang, G. Zeng, and A. Shakouri, Appl. Phys. Lett. **87**, 103506 (2005).

[49] J. Alvarez-Quintana, X. Alvarez, J. Rodriguez-Viejo, D. Jou, P. D. Lacharmoise, A. Bernardi, A. R. Goni, and M. I. Alonso, Appl. Phys. Lett. **93**, 013112 (2008).

[50] W. Kim and A. Majumdar, J. Appl. Phys. **99**, 084306 (2006).

[51] Y. K. Koh and D. G. Cahill, Phys. Rev. B **76**, 075207 (2007).

[52] I. Chowdhury, R. Prasher, K. Lofgreen, G. Chrysler, S. Narasimhan, R. Mahajan, D. Koester, R. Alley, and R. Venkatasubramanian, Nat. Nanotechnol. **4**, 235 (2009).